



1 Development and Testing of a Novel Sulfur Dioxide Sonde

2 Subin Yoon¹, Alexander Kotsakis^{1,2}, Sergio L. Alvarez¹, Mark G. Spychala^{3,4}, Elizabeth Klovenski¹, Paul
3 Walter³, Gary Morris^{3,5}, Ernesto Corrales⁶, Alfredo Alan⁶, Jorge Andres Diaz^{6,7}, James H. Flynn¹

4 ¹ Department of Earth and Atmospheric Sciences, University of Houston, Houston, TX, 77004, USA

5 ² now at ERT, Inc., Laurel, MD, 20707, USA

6 ³ St. Edward's University, Austin, TX, 78704, USA

7 ⁴ now at Hamelmann Communications, Pagosa Springs, CO, 81147, USA

8 ⁵ now at NOAA Global Monitoring Laboratory, Boulder, CO, 80305, USA

9 ⁶ GasLAB, CICANUM. Universidad de Costa Rica, San José, Costa Rica

10 ⁷ now at INFICON, East Syracuse, NY, 13057, United States

11

12

13 *Correspondence to:* James H. Flynn (jhflynn@central.uh.edu)

14



15 **Abstract.** A novel technique has been developed to measure sulfur dioxide (SO₂) using a modification of the existing
16 electrochemical concentration cell (ECC) ozonesonde technology. The current sonde-based method to measure SO₂ (i.e. the
17 dual-sonde approach) involves launching two ozonesondes together with one of the sondes having a filter to remove SO₂ at
18 the inlet. The SO₂ profile is determined by taking the difference between the measurements from the two instruments. The
19 dual-sonde method works well in typical tropospheric conditions when [O₃] > [SO₂] but saturates when [SO₂] > [O₃] and has
20 large uncertainties in the upper troposphere/lower stratosphere that would limit its effectiveness in measuring SO₂ from an
21 explosive volcanic eruption. Due to these limitations, several modifications were made to create a single-sonde system that
22 would directly measure SO₂ (i.e. the SO₂ sonde). These modifications included (1) a positively biased ECC background current,
23 (2) the addition of an O₃ removal filter, and (3) the addition of a sample dryer. The SO₂ sonde measures SO₂ as a reduction in
24 the cell current. There was a strong correlation ($r^2 > 0.94$) between the SO₂ sonde and a Thermo 43c analyzer during controlled
25 laboratory tests and pre-flight tests. Varying humidity levels affected the SO₂ sonde's sensitivity (84.6 ± 31.7 ppbv/ μ A, $1\sigma =$
26 37%) during initial field tests, which was resolved by adding a sample dryer upstream of the O₃ removal filter and pump inlet.
27 This modification significantly reduced the variability and increased the sensitivity of the SO₂ measurements (47 ± 5.8
28 ppbv/ μ A, $1\sigma = 12\%$). Field tests included measurements near Kilauea Volcano (before and during the 2018 eruption of the
29 Lower East Rift Zone), Costa Rica's Turrialba Volcano, and anthropogenic plumes from the Athabasca Oil Sands region of
30 Alberta, Canada. This single SO₂ sonde system is an effective, inexpensive instrument for measuring both ground-based and
31 vertical profiles of SO₂ from anthropogenic and natural sources (i.e. volcanic eruptions) over a wide range of concentrations.

32 **1 Introduction**

33 Sulfur dioxide (SO₂) emissions result from anthropogenic activities, such as power generation and crude oil refining processes,
34 and natural sources, such as volcanoes. In gas form, SO₂ acts as a respiratory irritant leading to complications with asthma and
35 cardiovascular conditions (Chen et al., 2007; Sunyer et al., 2003; Tzortziou et al., 2015, 2018). Gaseous SO₂ can be converted
36 to sulfate aerosols (Zhang et al., 2015), which are highly scattering, reduce visibility, and can have a cooling effect on the
37 climate when injected into the stratosphere (Kiehl and Briegleb, 1993; Schmidt et al., 2010). SO₂ acidifies rain, accelerating
38 damage of infrastructure and vegetation, particularly near SO₂ sources such as volcanoes (Delmelle et al., 2002; Krug and
39 Frink, 1983; Tortini et al., 2017). Due to these various climate, environmental, and human health-related impacts,
40 anthropogenic SO₂ has been heavily monitored (Shannon, 1999; Zhang and Schreifels, 2011), and regulations have been
41 enacted to reduce these emissions (EPA, 2000).

42
43 The largest natural sources of SO₂ are volcanoes. The eruption of Mt. Pinatubo in the Philippines in June 1991 had global
44 climatic effects and significant impacts on the tropospheric and lower stratospheric composition (Bluth et al., 1992; Parker et
45 al., 1996). Apart from such catastrophic eruptions, SO₂ can be continually emitted from volcanoes. SO₂ plumes from over 90
46 volcanoes have been reliably detected by satellites, resulting in the injection of an estimated 23 ± 2 Tg yr⁻¹ of SO₂ into the



47 atmosphere (Carn et al., 2017). However, unlike anthropogenic sources of SO₂, most volcanoes lack routine ground monitoring
48 (Galle et al., 2010; Pieri et al., 2013) and few opportunities exist for routine validation of satellite retrievals of SO₂ with *in situ*
49 measurements. Unmanned aerial vehicle (UAV) platforms can measure volcanic plumes at altitudes of 2 km above the take-
50 off altitude (Galle et al., 2010; Diaz et al., 2015). However, the lack and difficulty of monitoring and the possibility of another
51 stratospheric injection of SO₂ motivated the development of an inexpensive but reliable balloon-borne instrument that could
52 be deployed quickly after an eruption to validate satellite observations with *in situ* measurements.

53
54 Radiosondes and ozonesondes have been widely used for measurements of various atmospheric parameters (e.g. temperature,
55 air pressure, relative humidity [RH], and wind speed and direction) and O₃ concentrations, respectively. These measurements
56 produce vertical O₃ profiles and allow for the validation of satellite based O₃ vertical column density (VCD). The current
57 sonde-based method for measuring SO₂, the dual-sonde method, uses two En-Sci (Environmental Science Inc., Westminster,
58 CO) ozonesondes in tandem (Morris et al., 2010). For the dual-sonde method, an SO₂ removal filter is placed at the pump inlet
59 of one of the ozonesondes, scrubbing SO₂ from the sampled air before it enters the electrochemical concentration cell (ECC).
60 The other sonde samples unfiltered air (i.e. air containing both SO₂ and O₃). Due to the chemical reactions in the cathode cell,
61 the filtered sonde measures O₃, while the unfiltered sonde measures the difference between O₃ and SO₂ ([O₃] – [SO₂]) since
62 SO₂ has an equal (relative to O₃) but negative signal in the ECC (Morris et al., 2010). The SO₂ concentrations are then
63 determined from the difference between the two sonde measurements. This method works well in the troposphere when the
64 SO₂ concentration is less than the O₃ concentration, but not as well in intense plumes, such as those found in eruptive volcanic
65 environments. When the SO₂ concentration exceeds the O₃ concentration, the cell current in the unfiltered sonde becomes zero.
66 The excess SO₂ saturates the dual-sonde and distorts the calculated SO₂ profile. Additionally, in the stratosphere, where the
67 O₃ signal grows much larger than in the troposphere, the combined uncertainty of the measurements of the filtered and
68 unfiltered sondes results in a large lower limit of detection (LLOD), on the order of tens of ppbv. Thus, a field deployment of
69 the dual-sonde method more than a few days after an explosive, tropical volcanic eruption such as Mt. Pinatubo would result
70 in little useful data in the critical upper troposphere/lower stratosphere region.

71
72 This study reports on the development of a single instrument capable of *in situ* SO₂ measurements in the presence or absence
73 of O₃. This sonde can measure SO₂ at much greater concentrations than O₃ without saturating the system and can be configured
74 for a sub-ppbv LLOD (calculated using 3σ) at sea level. Since O₃ is removed from the sample stream, this SO₂ sonde avoids
75 the compounded errors of the dual-sonde method. Field deployments of the SO₂ sonde include sampling of volcanic emissions
76 from Kīlauea on the Big Island of Hawai'i, U.S., Turrialba Volcano in Costa Rica; and the emissions from petroleum extraction
77 and processing at the Athabasca Oil Sands, Canada. Results from these field tests, covering a wide range of SO₂ concentrations
78 from both natural and anthropogenic emission sources, are described below. The SO₂ sonde has been used for tethered and
79 free-release balloons but can also be adapted for UAV platforms.



80 2 Instrumentation

81 2.1 Ozonesondes

82 The standard and modified ECC En-Sci ozonesondes were used for the O₃ and SO₂ sonde measurements in this study. The
83 basic functioning of the ECC ozonesonde is described in Komhyr (1969) and Morris et al.(2010). The ECC sensor is composed
84 of platinum cathode and anode electrodes, each in its own cell, immersed in a diluted and saturated solution of potassium
85 iodide (KI), respectively. The cells are connected by an ion bridge allowing for the transfer of electrical charges while
86 maintaining the separation of the solutions (Eq. 1 and 2). When the cells are charged with the solution, a transient potential
87 difference is generated but dissipated through the redistribution of charge across the ion bridge. The following equilibria are
88 established from these reactions:



91

92 Sampled air is diffused into the cathode cell, and the presence of O₃ initiates a reaction (Eq. 3) that causes an imbalance in
93 favor of [I₂] in the cathode solution.



95 To rebalance the cell, the iodine/iodide redox reactions in Ep. 4 and 5 result in a flow of electrons from the anode to the cathode
96 via the ion bridge. This cell current, measured by an external ammeter, is proportional to the O₃ concentration.



99 As is also described in in Komhyr (1969) and Morris et al.(2010), when SO₂ is present in the sample air, an additional reaction
100 (Eq. 6) occurs in the cathode cell of the ECC, supplying the two electrons needed to rebalance the cathode cell after the O₃
101 reaction (Eq. 3).



103 Thus, each SO₂ molecule in the sampled air has the effect of cancelling the measurement of one O₃ molecule. In effect, the
104 standard ECC ozonesonde reports [O₃] - [SO₂] for its measurement. In most places and at most times, [SO₂] << [O₃], so there
105 is not a significant impact on the O₃ measurements, but in places downwind of SO₂ sources (e.g. coal-burning power plants or
106 volcanos), the O₃ measurement will be negatively impacted.



107 2.2 Instrumentation

108 Several SO₂ and O₃ instruments were used for validation of the SO₂ sonde during laboratory and field testing. A calibration
109 system was used to produce controlled concentrations of SO₂ and O₃. The calibration system relied on the operation of flow
110 controllers or restrictors, an SO₂ ultra-high purity (UHP) gas cylinder (4.87 ppm; Scott-Marrin, Inc., Riverside, CA) and/or a
111 U.V. Photometric O₃ calibrator (49C PS; Thermo Fisher Scientific, Franklin, MA), and zero air to produce desired pre-set
112 concentration of SO₂ and/or O₃. The zero-air setup used for the field and laboratory testing was achieved using a dry zero air
113 UHP gas cylinder or else generated by scrubbing ambient air through activated charcoal and Purafil SP (Purafil, Inc., Doraville,
114 GA) canisters. The Thermo 43i-TL SO₂ analyzer (LLOD: 60-90 pptv at 5 m averaging) and the 49i O₃ analyzer (LLOD: 1.5
115 ppbv at 5 m averaging) were also used during laboratory testing, while a Thermo 43c-TL SO₂ analyzer was used during field
116 testing in Hawai'i. These instruments were set to report 10 s average measurements.

117 3 Single-sonde SO₂ System and Laboratory Testing

118 3.1 SO₂ sonde system description

119 The first version (version 1.0) of the single-sonde SO₂ system (i.e. SO₂ sonde v1.0) included two major modifications to the
120 En-Sci ECC ozonesonde: (1) the application of a positively biased background current to the cathode cell and (2) the addition
121 of an O₃ removal filter. In a standard ECC, O₃ produces a positive response signal while SO₂ produces a negative signal when
122 sufficient O₃ (i.e. positive signal) is present. With these modifications, SO₂ can be measured directly as the reduction of the
123 cell current from the pre-set biased background current (Flynn and Morris, 2020). Unlike the dual-sonde system, this approach
124 allows for direct SO₂ measurements rather than an inference by subtraction of signals from two separate instruments. All
125 components of the SO₂ sonde fit within a standard ozonesonde foam box (approximately 8" x 8" x 10") except for the inlet
126 filter. The free-release balloon payload's total mass is approximately 1 kg. The patent publication provides a detailed
127 description and schematic of the SO₂ sonde (Flynn and Morris, 2020).

128 3.2 Testing of background current

129 The background bias current is supplied by inserting an additional platinum electrode in the cathode cell powered by a 9V
130 battery (Flynn and Morris, 2020). To maintain consistent power, the circuit uses a 5V regulator. Varying the resistor installed
131 in series with the battery and the electrode allows for a range of bias currents to be introduced. Laboratory tests compared the
132 SO₂ sonde measurements (initially configured without an O₃ removal filter) to those made by a 43i-TL SO₂ analyzer (Fig. 1,
133 Table 1). O₃ and SO₂ gases were introduced using the laboratory calibration setup and a manifold to allow the sonde and the
134 Thermo trace gas instruments to sample the same air. Results in Fig. 1 show 60 s averaged data. The test included (A) input of
135 O₃ without an added background current; (B) the same input of O₃ with the addition of a background current (equivalent to a
136 signal of approximately 90 ppbv); and the addition of SO₂ to the O₃ with the enhanced background signal where the SO₂



137 concentration was either (C) smaller or (D – E) larger than the O₃ concentration. During (A), measurements made by O₃ and
138 SO₂ sondes compare well to measurements made by the Thermo instruments (Fig.1, Table 1). The test included (E) the
139 response of the SO₂ sonde with a stepwise reduction of the O₃ concentration resulting in an equivalent decrease in signal,
140 followed by (G – I) a stepwise reduction in the SO₂ concentration resulting in an equivalent increase in signal. At (F), the SO₂
141 concentration exceeded the biased background current (90 ppbv), resulting in no sonde response. During the full test, the sonde
142 successfully measured SO₂ both with and without O₃ with approximately 97% efficiency.

143
144 Examination of the SO₂ sonde data showed that noise was proportional to the measured signal, with 1-σ noise at approximately
145 0.2 – 0.3% of the measured signal. Because increases in the SO₂ concentration result in a decrease in the signal (i.e. lower cell
146 currents), the magnitude of the applied background current bias determines the saturation point (i.e. upper limit of detection
147 [ULOD]) of the SO₂ sonde; saturation occurs when the measured cell current drops to zero. Applying a higher background
148 current increases the ULOD but also increases noise and the LLOD. During laboratory testing, the LLOD (3σ) was calculated
149 for a range of applied background current bias (0.25 to 10.0 μA). The LLOD for the varying bias current of 0.25 to 10.0 μA
150 ranged from approximately 0.002 to 0.084 μA, respectively.

151

152 **3.3 Testing of O₃ removal filter**

153 Since the ECC responds to both O₃ and SO₂, an O₃ removal filter was developed to remove interference from O₃ in the sample.
154 This proprietary O₃ removal filter is placed upstream of the sonde inlet (Flynn and Morris, 2020). During laboratory testing,
155 the O₃ removal filter was exposed to a continual concentration of 487 ± 3 ppbv of O₃ and a varying concentration of SO₂
156 ranging from 0 to 111 ± 1 ppbv (Fig. 2). The O₃ was effectively and consistently removed from the sampled air by the O₃
157 removal filter during a stepwise dilution of SO₂. The testing included measurements with (white background) and without
158 (gray background) the O₃ removal filter. The SO₂ and O₃ concentrations measured by the Thermo 43i-TL and 49i instruments,
159 respectively, and changes in SO₂ dilution levels are also indicated in Fig. 2. The O₃ removal filter destroyed the O₃ at all SO₂
160 dilution levels to below the detection limit of the O₃ instrument. By comparing the Thermo 43i-TL SO₂ analyzer measurements
161 with and without the O₃ removal filter, SO₂ passed through the filter with 88% efficiency (Fig. S1a). The transmission
162 efficiency was calculated by taking the ratio of SO₂ measured by the sonde to the analyzer. The SO₂ transmission efficiency
163 increased to 97% when testing the O₃ removal filter with the dry zero air UHP gas cylinder (Fig. S1b) instead of the zero air
164 generator that processes ambient laboratory air (Fig. S1a). Additional testing of the O₃ removal filter demonstrated that the
165 filter removed approximately 1 ppm of O₃ at sea level with > 99.9% efficiency, below the detection limit of the Thermo 49i
166 O₃ monitor.

167



168 4. Field Deployments, Part I

169 This SO₂ sonde (SO₂ sonde v1.0) was deployed and tested in Hawai'i and Costa Rica (Fig. S2). The field sites were close to
170 active volcanoes, which are significant sources of natural SO₂ (Tang et al., 2020; Carn et al., 2017). In Hawai'i, field
171 measurements were made near Kīlauea Volcano on the south-eastern shore of Island of Hawai'i, the largest of Hawai'i's islands.
172 Kīlauea is the youngest volcano on the island and one of Earth's most active volcanoes (Kern et al., 2015; Nadeau et al., 2015).
173 Kīlauea had been in a state of eruption since 1983 (Patrick et al., 2019) with an average SO₂ release rate of approximately
174 5,500 T/d measured during 2014 – 2017 (Elias et al., 2018). In Costa Rica, field measurements were made near Turrialba
175 Volcano, one of the most active volcanoes in the Central American Volcanic Arc. Studies of emissions from Turrialba prior
176 to 2013 reported SO₂ release rates of up to 4,000 T/d (de Moor et al., 2016; Xi et al., 2016). Activity escalated after 2014,
177 raising concerns for air quality and environmental health (de Moor et al., 2016; Tortini et al., 2017).

178 4.1 Kīlauea, Hawai'i - February 2018

179 The first deployment of the SO₂ sonde v1.0 was during NASA's HypIRI HyTES Hawaii Campaign (H3C) from February 3-
180 10, 2018, near Kīlauea Volcano. The instrument was tested in flights on free-release and a tethered balloon system (TBS), and
181 at ground level with measurements in Hawaii Volcanoes National Park (HVNP) downwind of Kīlauea's summit crater,
182 Halema'uma'u. During the ground-level testing, an SO₂ sonde and a Thermo 43c-TL SO₂ analyzer's sample inlet were mounted
183 on the top of a van for co-located sampling.

184
185 Figure 3a depicts the measurements taken during the first encounter with an SO₂ plume while driving through the HVNP on
186 February 3, 2018. The strongly correlated SO₂ sonde and Thermo 43c-TL measurements ($r^2 = 0.99$) reached upward of ~940
187 ppbv. The SO₂ sonde had a sensitivity of 118.4 ± 0.4 ppbv/ μ A, determined by regression analysis of the sonde's cell current
188 with the Thermo 43c-TL concentrations (Fig. 3a). SO₂ sonde sensitivity varied significantly during the field deployment.
189 During surface measurements on February 10, 2018, earlier zero-air calibrations measured a sensitivity of 86.5 ± 1.5 ppbv/ μ A
190 while measurements during a SO₂ plume event, with peak concentrations of up to 400 ppbv, the SO₂ sonde's sensitivity was
191 73.9 ± 0.6 ppbv/ μ A (Fig. 3b). Although the SO₂ sonde sensitivity varied significantly in ten subsequent calibrations ($84.6 \pm$
192 31.7 ppbv/ μ A), the measurements remained strongly correlated (range: $r^2 = 0.94 - 0.99$). The variability in the sensitivity in
193 the field was likely due to changes in the ambient RH impacting the SO₂ transmission efficiency of the O₃ removal filter. This
194 hypothesis was further confirmed by laboratory RH testing and discussed in Sect. 5.

195 4.2 Turrialba, Costa Rica (Dual-sonde versus SO₂ sonde comparison)

196 On March 23, 2018, the University of Houston/St. Edward's University team conducted a free release flight from the
197 Universidad de Costa Rica's campus in San Jose (approximately 31 km downwind of Turrialba Volcano) consisting of a
198 traditional SO₂ dual-sonde payload (Morris et al., 2010) as well as the SO₂ sonde v1.0. This flight provided the first direct *in*



199 *situ* comparison of the two SO₂ sonde methods. Figure 4 shows the response of the SO₂ sonde v1.0 and the calculated SO₂
200 dual-sonde profile. The dual-sonde SO₂ method can only report concentrations of SO₂ up to a maximum of the concentration
201 of O₃ present. Furthermore, because the SO₂ concentration is determined by subtracting the signals from two instruments, its
202 uncertainty is higher than the uncertainty of a measurement from a single instrument. When [SO₂] > [O₃], the dual sonde's
203 unfiltered ozonesonde signal goes to zero, as happened for the Turrialba sonde launch between 3 – 5 km (Fig. 4). The SO₂
204 saturates the cathode solution in the unfiltered sonde, not recovering until enough ambient O₃ has been processed to rebalance
205 the cell, resulting in a distorted profile (Fig. 4). For this flight, the SO₂ sonde was configured to its maximum range (ULOD of
206 approximately 450 ppbv) and was able to capture both the small plume below 2 km above mean sea level (AMSL)
207 (approximately 18 ppbv) as well as the primary plume between 3 – 4 km AMSL (approximately 230 ppbv). The SO₂ sonde
208 v1.0 was able to capture the full shape of the profile, including the peak values and structure of the plume. The SO₂ sonde v1.0
209 reports the top of the plume around 4 km AMSL, whereas the dual-sonde remains saturated until closer to 5 km AMSL. Thus,
210 the dual-sonde SO₂ profiles, when saturated by high concentrations of SO₂, erroneously appear to have a greater vertical extent.
211 Further, the SO₂ sonde v1.0 showed no interference from O₃ from the surface to altitude at 24.4 km AMSL, with O₃
212 concentrations in the stratospheric O₃ layer reaching > 4 ppmv (not shown), demonstrating the effectiveness of the O₃ filter.
213 The SO₂ VCD was 8.3 DU (Dobson Units, 1 DU = 2.69 × 10¹⁶ molecules cm⁻²) for the SO₂ sonde but was only 3.4 DU for the
214 dual-sonde measurement. Thus, once saturated, the dual-sonde method may underestimate the SO₂ VCD. Additional laboratory
215 testing is planned to resolve this discrepancy.

216 5. Post Field Test Improvements and Laboratory Testing

217 The variability in the SO₂ sonde v1.0's sensitivity during the initial field tests was hypothesized to be due to varying levels of
218 humidity. SO₂ is soluble in water and through multiphase reactions can be oxidized to sulfuric acid in the atmosphere in the
219 presence of water vapor (e.g. precipitation, clouds, fog, etc.) (Carmichael and Peters, 1979; Zhang et al., 2013; Terraglio and
220 Manganeli, 1967). Factors including liquid water content, aerosol composition, aerosol loading, and pH of the water are
221 important in determining adsorption and oxidation rate of SO₂ (Liu et al., 2021). With increased humidity and presence of a
222 filter, SO₂ gas is likely adsorbing on the filter causing lower SO₂ transmission efficiency due to potential uptake of SO₂ in
223 water on the filter. Several laboratory tests were done to confirm the need to remove water from the sample upstream of the
224 O₃ removal filter. A desiccant membrane dryer (Perma Pure LLC, Lakewood, NJ) composed of a Nafion™ tube in silica gel
225 desiccant was placed in-line upstream of the O₃ removal filter. This sample dryer is lightweight, relatively inexpensive, and
226 does not require power.

227
228 Laboratory tests included exposing the SO₂ sonde, with and without a sample dryer, to controlled levels of humidity and SO₂.
229 Without removing water vapor, the SO₂ transmission efficiency decreases as humidity increases, particularly above 50% RH
230 (Fig. 5). As the O₃ removal filter is humidified, the SO₂ transmission efficiency decreases due to increased SO₂ loss in the



231 filter. With the sample dryer in place, the SO₂ transmission efficiency varies by an average of <1% across a range of 0-85%
232 RH (Fig. 5).

233
234 The dryer's useful lifetime was determined by continuously exposing it to high humidity (> 95% RH at approximately 23 °C)
235 sample stream. The downstream RH climbed from 5% to 16% after 2.3 h and to 25% after 6.3 h. At these downstream RH
236 levels, the SO₂ transmission efficiency remained above 95%. A typical SO₂ sonde's measurement time per flight, including
237 pre-flight calibration, is approximately three hours. The dryer's useful lifetime is likely much longer than required for a flight
238 since exposure to 95% RH conditions for several hours is highly unusual outside of hurricanes and tropical systems for balloon
239 measurements. SO₂ sonde and Thermo 43c-TL measurements were strongly correlated ($r^2 = 0.99$) during a multipoint
240 calibration conducted using the O₃ removal filter and the dryer under relatively high humidity levels. During that calibration,
241 the SO₂ sonde's sensitivity was 45.43 ± 0.17 ppbv/ μ A. By comparison, the average sensitivity during the H3C campaign was
242 84.6 ± 31.7 ppbv/ μ A across 10 sondes. The sample dryer, therefore, improved both the sensitivity and stability of the
243 measurements observed.

244

245 **6 Field Deployments, Part II**

246 The updated SO₂ sonde (SO₂ sonde v1.1) with the dryer filter was deployed and tested in Ft. McMurray, Canada, and again in
247 Hawai'i in June 2018. Ft. McMurray is in the Alberta province of Canada and is home to the Athabasca Oil Sands, a large area
248 of bitumen and heavy crude oil surface deposits high in sulfur content. Local processing of these products (e.g. surface mining)
249 and resulting by-products (e.g. tailing ponds) can release significant amounts of SO₂ into the atmosphere (Bari et al., 2020;
250 McLinden et al., 2016; Simpson et al., 2010). A second field deployment to Hawai'i followed immediately after the deployment
251 to Canada. On May 3, 2018, Kīlauea Volcano on Hawai'i entered a new eruptive phase with an outbreak of a series of fissures
252 in the lower Puna area (Liu et al., 2021; Anderson et al., 2019; Gansecki et al., 2019; Patrick et al., 2020). The active phase
253 volcanic gas emissions resulted in localized evacuations in the Lower East Rift Zone (LERZ) and poor air quality for much of
254 the southern and western portions of the island (Tang et al., 2020). The eruption event entered a paused phase in early August,
255 and was declared over on December 5, 2018 (Kern et al., 2020).

256 **6.1 Athabasca Oil Sands, Canada**

257 The SO₂ sonde v1.1 was tested in Ft. MacKay (near Ft. McMurray; 57.1206° N, 111.4241° W), Alberta, in the Athabasca Oil
258 Sands from June 10 – 16, 2018 (Fig. S2c). This field project, conducted in conjunction with Environment Canada and York
259 University, evaluated SO₂ emissions from industrial activities in and near the oil sands region using a combination of TBS and
260 ground-based measurements. The SO₂ sonde v1.1 was flown on the York TBS payload recording measurements from the
261 ground to 300 m above ground level (AGL; 650 m AMSL). This deployment provided a dilute anthropogenic plume to test



262 the SO₂ sonde in a high-sensitivity, low-range configuration. The average sensitivity of the SO₂ sonde v1.1 during the project
263 was 51 ± 1.2 ppbv/ μ A. The SO₂ sonde was configured to sample in a range from ~ 0.5 -25 ppbv of SO₂. The TBS SO₂ sonde's
264 vertical profiles were averaged into 10 m altitude bins that measured SO₂ concentration ranges that are more representative of
265 anthropogenically-impacted SO₂ rather than large volcanic plumes (Fig. 6). This field deployment also demonstrated the
266 performance of the sonde at sub-ppbv levels of ambient SO₂.

267 **6.2. Kīlauea, Hawai'i - June 2018**

268 In response to the larger eruption that started in May 2018, the SO₂ sonde v1.1 was deployed to Hawai'i for the NASA-funded
269 Big Island SO₂ Survey (BISOS). The SO₂ sonde launches occurred from Kahuku Ranch (19.0549° N, 155.6934° W) and
270 Na'alehu Elementary School (19.0610° N, 155.5788° W) approximately 90 km downwind of Kīlauea's LERZ (Fig. S2d). The
271 site's distance from the source allowed the plume to disperse and dilute as compared with measurements at the vent. An SO₂
272 plume was detected during seven of the nine free-release balloon launches during the June 2018 BISOS campaign. The ten
273 SO₂ sonde v1.1 calibrations performed during BISOS had an SO₂ sensitivity of 47.0 ± 5.8 ppbv/ μ A and were similar to the
274 laboratory results using dry air (45.43 ± 0.17 ppbv/ μ A).

275
276 With the anticipated levels of SO₂, the sondes were configured to sample at the maximum range of 10-450 ppbv of SO₂.
277 Figure 7 shows four distinctive SO₂ profiles, and Table 2 includes the VCDs for each flight. No plumes above 5 km AMSL
278 were detected, at which point reductions in air density significantly impacted the LLOD. All but one of the observed SO₂
279 plumes were below the capping inversion of the planetary boundary layer (PBL). On June 22 (Fig. 7a), the ascent profile
280 shows SO₂ below 3 km AMSL peaking at nearly 100 ppbv and additional features between 3-4 km AMSL peaking at 20-35
281 ppbv (Tang et al., 2020). The latter peaks were correlated with higher RH, perhaps the result of steam from a vent or the
282 ocean entry points having broken through the inversion. The early afternoon June 28 profile (Fig. 7b) shows the highest
283 concentration (325 ppbv) for a resolved SO₂ plume during the BISOS campaign. Typical for the trade winds, HYSPLIT
284 trajectories showed the winds were out of the NE, consistent with the plume's transport from vents in the LERZ or the lava
285 ocean entry points. Although the descent profile from a June 29 early afternoon launch lost the signal at 0.58 km AMSL, Fig.
286 7c shows an SO₂ plume over the ocean with a peak concentration of 188 ppbv at 0.74 km AMSL. HYSPLIT trajectories
287 again showed the winds were out of the NE. Lastly, the SO₂ plume detected during the ascent of the June 30 launch (Fig. 7d)
288 exceeded the ULOD between 1-3 km AMSL for the SO₂ sonde configuration used. The distorted SO₂ enhancement
289 extending above the PBL as determined by the temperature inversion is most likely an artifact of the saturated sonde, similar
290 to what was seen in the dual-sonde profile from Costa Rica (Fig. 4). As the RH remains low above the PBL, it is most likely
291 that the SO₂ is contained entirely within the PBL.



292 5. Conclusion and Future Work

293 An innovative new method for measuring vertical profiles of SO₂ from TBS and free-release balloons was successfully tested
294 and demonstrated in controlled laboratory experiments and during four different field deployments covering SO₂
295 concentrations ranging from 0.5-325 ppbv during flights and up to 940 ppbv during ground measurements. This new method
296 requires three major modifications to the standard ECC ozonesonde: the addition of a positive background current, an O₃
297 removal filter, and a sample dryer. Relative to the previous dual-sonde method, the new method measures SO₂ using a single-
298 sonde system (i.e. the SO₂ sonde). The SO₂ sonde and Thermo 43c-TL measurements were strongly correlated during
299 laboratory ($r^2 > 0.99$) and field-based ($r^2 > 0.94$) comparisons. Initial field tests and subsequent laboratory testing of SO₂ sonde
300 v1.0 highlighted the need to dry the sample upstream of the O₃ removal filter to achieve consistent results. Follow-up field
301 measurements in the Athabasca Oil Sands and Hawai'i clearly demonstrated the improvement in the SO₂ sonde v1.1's
302 sensitivity and consistency (51 ± 1.2 and 47 ± 5.8 ppbv/ μ A, respectively) as a result of drying the sample.

303
304 The SO₂ sonde v1.1 offers several advantages over the dual-sonde method, including the ability to measure [SO₂] independent
305 of [O₃], the capability of sub-ppbv detection limits, faster response and recuperation time when exposed to larger SO₂ plumes,
306 and reduced uncertainty. The lighter weight of the payload requires a smaller balloon and less helium to lift, which may prove
307 advantageous for deployment under some field conditions, particularly where helium supplies are limited. It's compactness
308 and weight can also make it a candidate for small drones and UAV campaigns. Field deployments revealed specific issues and
309 areas for improvement. The present design requires pre-setting the sonde's background current prior to the launch. Thus, some
310 *a priori* estimates of the plume are required to determine the appropriate background current so that the instrument can measure
311 the full range of SO₂ concentrations present. In the current SO₂ sonde v1.1, increasing the ULOD by applying a larger
312 background current also increases the LLOD. Further laboratory experiments are needed to identify the factors that cause the
313 remaining observed variability in the SO₂ transmission efficiency in the latest instrument version that includes the sample
314 dryer. Much of the testing and calibration completed to date assessed the complete SO₂ sonde system (i.e. sonde, filter, dryer).
315 Building a database of the various individual factors, including pump speeds and filter transmission efficiency, will better
316 characterize the causes of sonde-to-sonde variability and allow future versions of the system to improve performance
317 characteristics so that the system can be made available for operational use.

318 Author Contributions

319 Conceptualization by J.H.F. and G.M. Data curation by J.H.F., A.K., S.L.A., M.G.S., E.K., P.W., G.M., E.C., A.A., and J.A.D.
320 Formal analysis by A.K., S.L.A., S.Y. and P.W. Funding acquisition by J.H.F. Investigation by A.K., S.L.A., M.G.S., and E.K.
321 Methodology by J.H.F. and G.M. Writing – original draft preparation by S.Y. Writing – review and editing by P.W. G.M.,
322 J.A.D. and J.H.F. Supervision by J.H.F.

323



324 **Conflict of Interest:** The authors declare that they have no conflict of interest.

325 **Acknowledgments**

326 This work was supported by NASA grant numbers NNG11HP16A and 80NSSC18K1061. We especially appreciate our
327 collaboration with En-Sci in advancing this work. We would also like to thank Mark Gordon of York University and David
328 Tarasick of Environment Canada for their invitation and assistance with the deployment to Ft. McMurray, to Henry Selkrik
329 and Holger Vomel from the TicoSonde Project for their support in the Turrialba Volcano testing campaign. A special thanks
330 to Principal Darlene Javar of Na'alehu Elementary School and its teachers, staff, and students for letting us install equipment
331 on a roof and helping us with a launch.
332



333

334

335 **Table 1: Averaged O₃ and SO₂ concentration measured by the SO₂ sonde version 1.0 and Thermo instruments during different**
 336 **stages of testing indicated in Fig. 1.**

	O ₃ Thermo (ppbv)	O ₃ Sonde (ppbv)	SO ₂ Thermo (ppbv)	SO ₂ Sonde (ppbv)
A	103 ± 0.4	100 ± 1.3	-0.3 ± 0.06	99 ± 1.8
B	104 ± 0.5	102 ± 0.4	-0.4 ± 0.06	190 ± 2.3
C	103 ± 0.4	100 ± 0.4	57 ± 0.40	138 ± 1.0
D	103 ± 0.5	98 ± 0.6	116 ± 1.9	81 ± 1.0
E	-	-	-	-
F	-0.13 ± 0.5	0.53 ± 0.2	116 ± 1.4	5.3 ± 0.1
G	-0.44 ± 0.4	0	58 ± 0.7	30 ± 0.6
H	-1.0 ± 0.4	0.40 ± 0.04	24 ± 0.8	67 ± 0.8
I	-1.3 ± 0.29	1.12 ± 0.28	-0.25 ± 0.22	91 ± 0.7

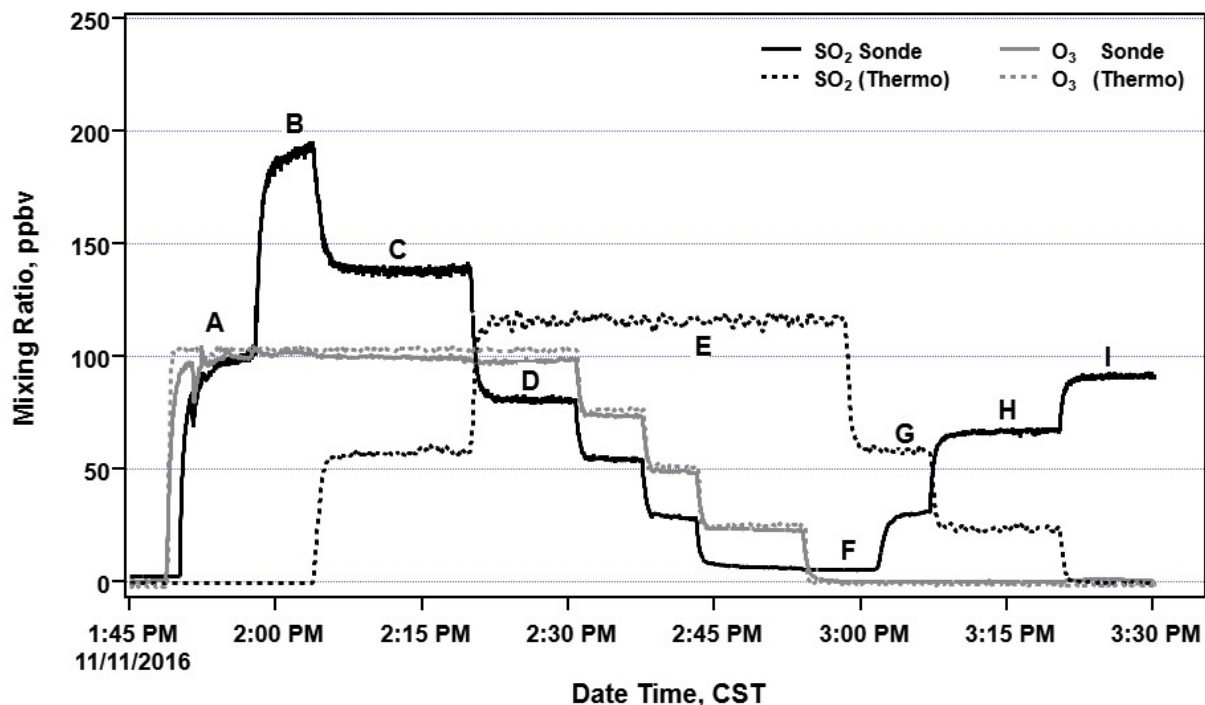
337

338 **Table 2. The SO₂ vertical column density (VCD) for profiles shown in Fig. 7 from BISOS in June 2018. For profile c, the descent**
 339 **profile VCD is reported for the flight without extrapolation (shown without parentheses) and using linear extrapolation assuming**
 340 **the SO₂ concentration to be 0 ppbv at sea level (shown in parentheses).**

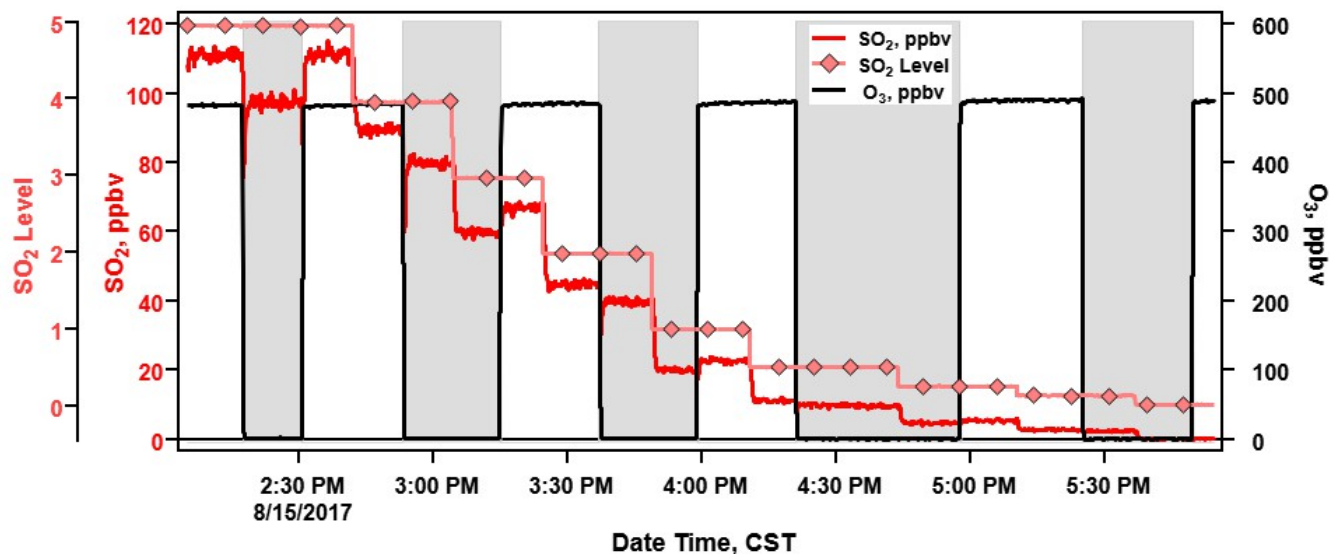
Profile	Launch Time (UTC)	SO ₂ VCD
a (ascent)	06/22/2018 00:32	8.6 DU
b (ascent)	06/28/2018 20:45	12.5 DU
c (descent)	06/29/2018 21:36	6.2 (9.8*) DU
d (ascent)	06/30/2018 20:48	79.1 DU**

* VCD from extrapolated data

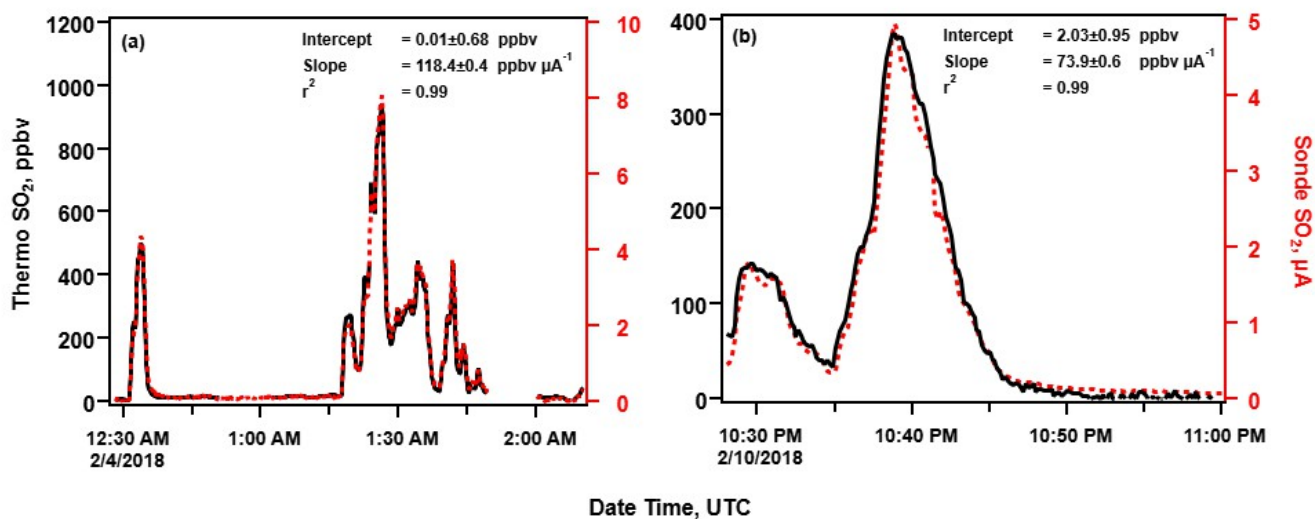
** Saturation of SO₂ at altitudes of 1 to 3 km AMSL



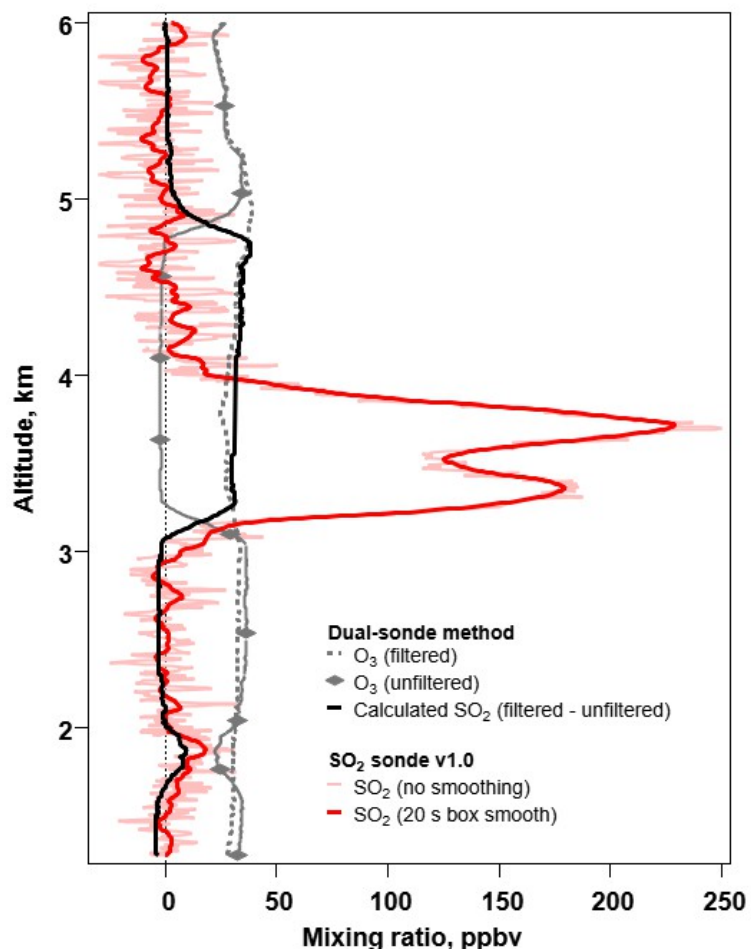
342 Figure 1: Test of the SO₂ sonde v1.0 (without an O₃ removal filter) with an applied background current responding to O₃ and SO₂.
 343 See the text for further details.



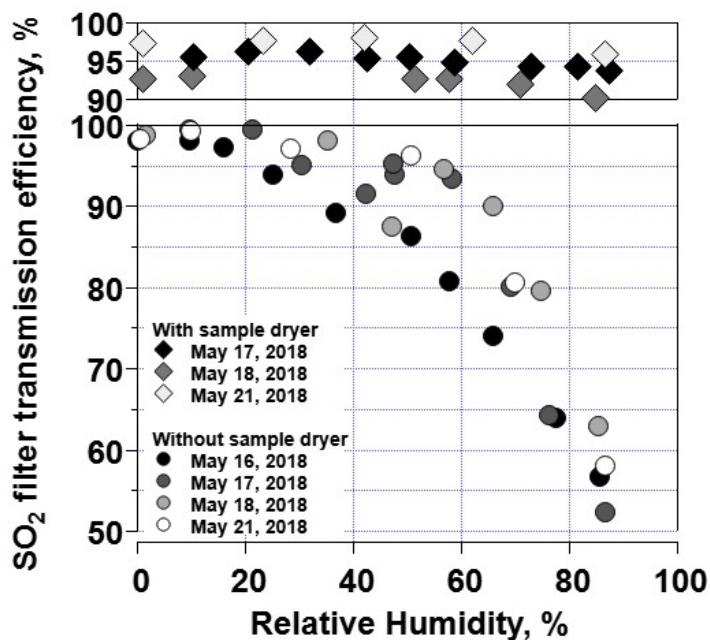
345 Figure 2: Time of series of a multipoint test of O₃ filter removal efficiency and impact on SO₂ measurements taken by a Thermo 43i-
 346 TL SO₂ analyzer. Changes in SO₂ dilution levels are indicated by the blue lines.



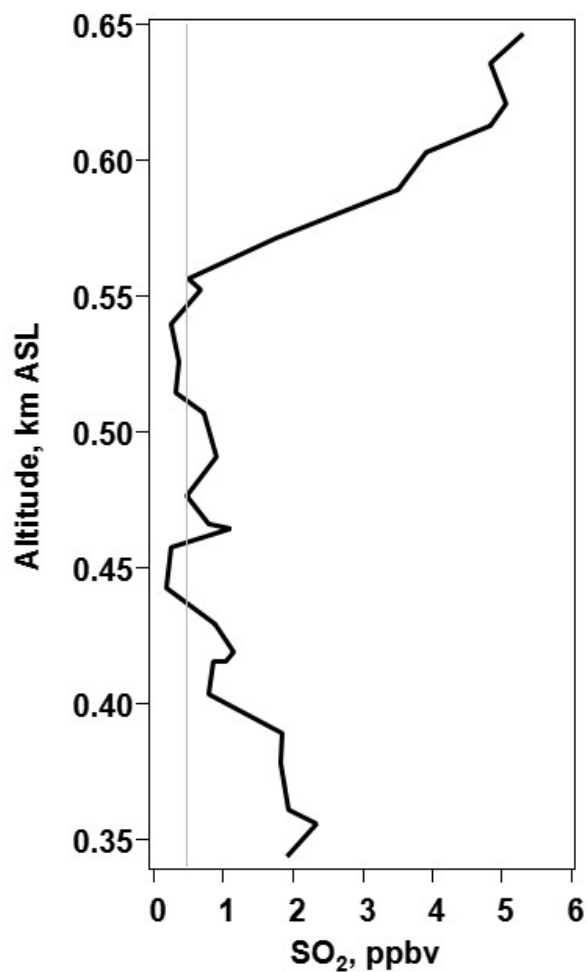
348 Figure 3: SO₂ sonde v1.0 and Thermo Environmental SO₂ analyzer measurements at Kilauea, Hawai'i during H3C for (a) initial
349 SO₂ plume encounter on February 3, 2018, and (b) a pre-flight measurement on February 10, 2018, approximately 6 km downwind
350 of Kilauea's summit crater.



352 Figure 4: The profiles of a triple-sonde payload, which consisted of a dual-sonde in tandem with an SO₂ sonde v1.0, launched from
353 the Universidad de Costa Rica's campus in San Jose (approximately 31 km downwind of the volcano Turrialba) on March 23, 2018.

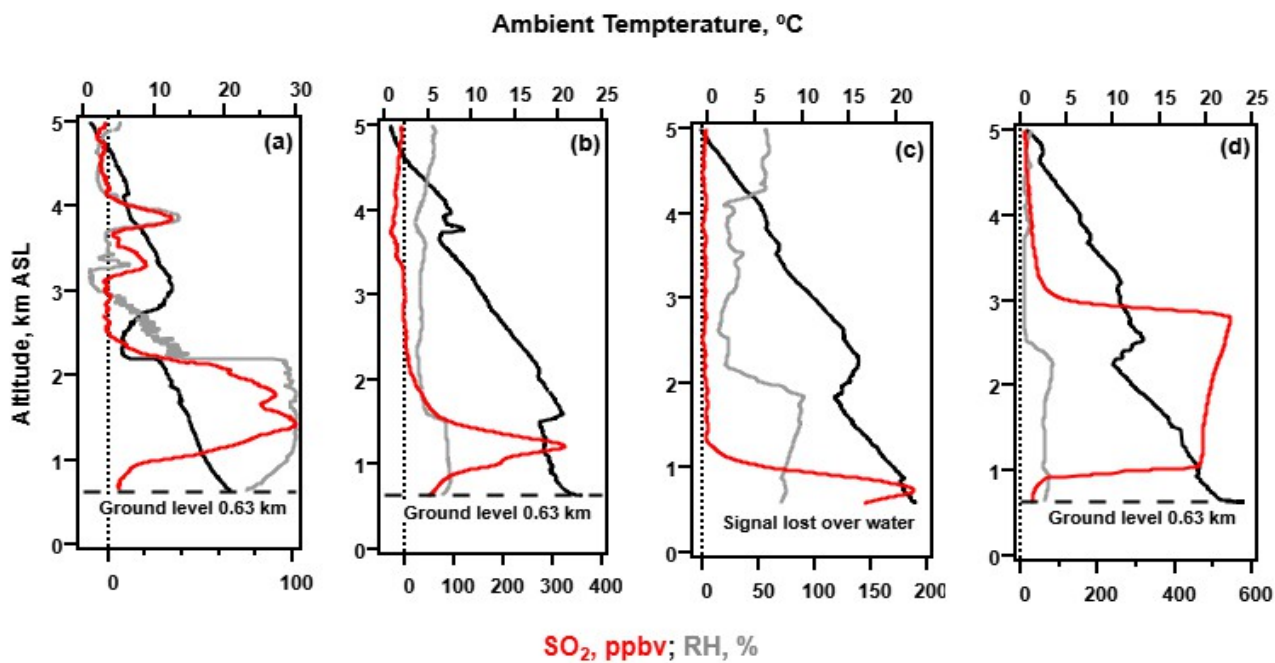


355 Figure 5: Tests of SO₂ transmission efficiency as a function of relative humidity without (circles) and with an upstream sample dryer
356 (diamonds).



358 Figure 6: The profile, constructed using 20 s average changes in altitude (ranging from 1 to 15 km), is for a tethered SO₂ sonde v1.1
359 in the Athabasca Oil Sands region of Alberta, Canada. The SO₂ sonde background current was 0.5 μ A, and the LLOD was 0.47
360 ppbv.

361



363 Figure 7: Vertical profiles of SO₂ (20 s box smoothing) from the SO₂ sonde v1.1 during BISOS in June 2018 with free-release balloon
364 launches occurring at the Kahuku Ranch on the Big Island of Hawai'i. Profiles are from (a) 6/22/2018 00:32; (b) 6/28/2018 20:45; (c)
365 6/29/2018 21:36; and (d) 6/30/2018 20:48. All times are UTC.

366



367 References

- 368 Anderson, K. R., Johanson, I. A., Patrick, M. R., Gu, M., Segall, P., Poland, M. P., Montgomery-Brown, E. K., and Miklius,
369 A.: Magma reservoir failure and the onset of caldera collapse at Kīlauea Volcano in 2018, *Science*, 366, 2019.
- 370 Bari, M. A., Kindzierski, W. B., and Roy, P.: Identification of ambient SO₂ sources in industrial areas in the lower Athabasca
371 oil sands region of Alberta, Canada, *Atmospheric Environment*, 231, 117505, 2020.
- 372 Bluth, G. J., Doiron, S. D., Schnetzler, C. C., Krueger, A. J., and Walter, L. S.: Global tracking of the SO₂ clouds from the
373 June, 1991 Mount Pinatubo eruptions, *Geophysical Research Letters*, 19, 151–154, 1992.
- 374 Carmichael, G. R. and Peters, L. K.: Some aspects of SO₂ absorption by water-generalized treatment, *Atmospheric
375 Environment* (1967), 13, 1505–1513, 1979.
- 376 Carn, S., Fioletov, V., McLinden, C., Li, C., and Krotkov, N.: A decade of global volcanic SO₂ emissions measured from
377 space, *Scientific reports*, 7, 1–12, 2017.
- 378 Chen, T.-M., Kuschner, W. G., Gokhale, J., and Shofer, S.: Outdoor air pollution: nitrogen dioxide, sulfur dioxide, and carbon
379 monoxide health effects, *The American journal of the medical sciences*, 333, 249–256, 2007.
- 380 Delmelle, P., Stix, J., Baxter, P., Garcia-Alvarez, J., and Barquero, J.: Atmospheric dispersion, environmental effects and
381 potential health hazard associated with the low-altitude gas plume of Masaya volcano, Nicaragua, *Bulletin of Volcanology*,
382 64, 423–434, 2002.
- 383 Diaz, J. A., Pieri, D., Wright, K., Sorensen, P., Kline-Shoder, R., Arkin, C. R., Fladeland, M., Bland, G., Buongiorno, M. F.,
384 and Ramirez, C.: Unmanned aerial mass spectrometer systems for in-situ volcanic plume analysis, *Journal of the American
385 Society for Mass Spectrometry*, 26, 292–304, 2015.
- 386 Elias, T., Kern, C., Horton, K. A., Sutton, A. J., and Garbeil, H.: Measuring SO₂ emission rates at Kīlauea Volcano, Hawaii,
387 using an array of upward-looking UV spectrometers, 2014–2017, *Frontiers in Earth Science*, 6, 214, 2018.
- 388 EPA: National Air Pollutant Emission Trends, 2000.
- 389 Flynn, J. and Morris, G. A.: A method for directly measuring so₂ and other trace gases by electrochemical cell (ecc) sonde,
390 2020.
- 391 Galle, B., Johansson, M., Rivera, C., Zhang, Y., Kihlman, M., Kern, C., Lehmann, T., Platt, U., Arellano, S., and Hidalgo, S.:
392 Network for Observation of Volcanic and Atmospheric Change (NOVAC)—A global network for volcanic gas monitoring:
393 Network layout and instrument description, *Journal of Geophysical Research: Atmospheres*, 115, 2010.
- 394 Gansecki, C., Lee, R. L., Shea, T., Lundblad, S. P., Hon, K., and Parcheta, C.: The tangled tale of Kīlauea’s 2018 eruption as
395 told by geochemical monitoring, *Science*, 366, 2019.
- 396 Kern, C., Sutton, J., Elias, T., Lee, L., Kamibayashi, K., Antolik, L., and Werner, C.: An automated SO₂ camera system for
397 continuous, real-time monitoring of gas emissions from Kīlauea Volcano’s summit Overlook Crater, *Journal of Volcanology
398 and Geothermal Research*, 300, 81–94, 2015.



- 399 Kern, C., Lerner, A. H., Elias, T., Nadeau, P. A., Holland, L., Kelly, P. J., Werner, C. A., Clor, L. E., and Cappos, M.:
400 Quantifying gas emissions associated with the 2018 rift eruption of Kīlauea Volcano using ground-based DOAS
401 measurements, *Bulletin of Volcanology*, 82, 1–24, 2020.
- 402 Kiehl, J. and Briegleb, B.: The relative roles of sulfate aerosols and greenhouse gases in climate forcing, *Science*, 260, 311–
403 314, 1993.
- 404 Komhyr, W.: Electrical concentration cells for gas analysis, *Ann. Geophys.*, 25, 203–210, 1969.
- 405 Krug, E. C. and Frink, C. R.: Acid rain on acid soil: a new perspective, *Science*, 221, 520–525, 1983.
- 406 Liu, T., Chan, A. W., and Abbatt, J. P.: Multiphase Oxidation of Sulfur Dioxide in Aerosol Particles: Implications for Sulfate
407 Formation in Polluted Environments, *Environmental Science & Technology*, 55, 4227–4242, 2021.
- 408 McLinden, C. A., Fioletov, V., Krotkov, N. A., Li, C., Boersma, K. F., and Adams, C.: A decade of change in NO₂ and SO₂
409 over the Canadian oil sands as seen from space, *Environmental science & technology*, 50, 331–337, 2016.
- 410 de Moor, J. M., Aiuppa, A., Avard, G., Wehrmann, H., Dunbar, N., Muller, C., Tamburello, G., Giudice, G., Liuzzo, M., and
411 Moretti, R.: Turmoil at Turrialba Volcano (Costa Rica): Degassing and eruptive processes inferred from high-frequency gas
412 monitoring, *Journal of Geophysical Research: Solid Earth*, 121, 5761–5775, 2016.
- 413 Morris, G. A., Komhyr, W. D., Hirokawa, J., Flynn, J., Lefer, B., Krotkov, N., and Ngan, F.: A balloon sounding technique
414 for measuring SO₂ plumes, *Journal of Atmospheric and Oceanic Technology*, 27, 1318–1330, 2010.
- 415 Nadeau, P. A., Werner, C. A., Waite, G. P., Carn, S. A., Brewer, I. D., Elias, T., Sutton, A. J., and Kern, C.: Using SO₂ camera
416 imagery and seismicity to examine degassing and gas accumulation at Kīlauea Volcano, May 2010, *Journal of Volcanology
417 and Geothermal Research*, 300, 70–80, 2015.
- 418 Parker, D. E., Wilson, H., Jones, P. D., Christy, J., and Folland, C. K.: The impact of Mount Pinatubo on world-wide
419 temperatures, *International Journal of Climatology: A Journal of the Royal Meteorological Society*, 16, 487–497, 1996.
- 420 Patrick, M., Orr, T., Anderson, K., and Swanson, D.: Eruptions in sync: Improved constraints on Kīlauea Volcano’s hydraulic
421 connection, *Earth and Planetary Science Letters*, 507, 50–61, 2019.
- 422 Patrick, M., Johanson, I., Shea, T., and Waite, G.: The historic events at Kīlauea Volcano in 2018: summit collapse, rift zone
423 eruption, and M w 6.9 earthquake: preface to the special issue, 2020.
- 424 Pieri, D., Diaz, J. A., Bland, G., Fladeland, M., Madrigal, Y., Corrales, E., Alegria, O., Alan, A., Realmuto, V., and Miles, T.:
425 In situ observations and sampling of volcanic emissions with NASA and UCR unmanned aircraft, including a case study at
426 Turrialba Volcano, Costa Rica, *Geological Society, London, Special Publications*, 380, 321–352, 2013.
- 427 Schmidt, A., Carslaw, K., Mann, G., Wilson, M., Breider, T., Pickering, S., and Thordarson, T.: The impact of the 1783–1784
428 AD Laki eruption on global aerosol formation processes and cloud condensation nuclei, *Atmospheric Chemistry and Physics*,
429 10, 6025–6041, 2010.
- 430 Shannon, J. D.: Regional trends in wet deposition of sulfate in the United States and SO₂ emissions from 1980 through 1995,
431 *Atmospheric Environment*, 33, 807–816, 1999.



- 432 Simpson, I., Blake, N., Barletta, B., Diskin, G., Fuelberg, H., Gorham, K., Huey, L., Meinardi, S., Rowland, F., and Vay, S.:
433 Characterization of trace gases measured over Alberta oil sands mining operations: 76 speciated C 2–C 10 volatile organic
434 compounds (VOCs), CO 2, CH 4, CO, NO, NO 2, NO y, O 3 and SO 2, *Atmospheric Chemistry and Physics*, 10, 11931–
435 11954, 2010.
- 436 Sunyer, J., Atkinson, R., Ballester, F., Le Tertre, A., Ayres, J. G., Forastiere, F., Forsberg, B., Vonk, J., Bisanti, L., and
437 Anderson, R.: Respiratory effects of sulphur dioxide: a hierarchical multicity analysis in the APHEA 2 study, *Occupational
438 and Environmental Medicine*, 60, e2–e2, 2003.
- 439 Tang, Y., Tong, D. Q., Yang, K., Lee, P., Baker, B., Crawford, A., Luke, W., Stein, A., Campbell, P. C., and Ring, A.: Air
440 quality impacts of the 2018 Mt. Kilauea Volcano eruption in Hawaii: A regional chemical transport model study with satellite-
441 constrained emissions, *Atmospheric Environment*, 237, 117648, 2020.
- 442 Terraglio, F. P. and Manganeli, R. M.: The absorption of atmospheric sulfur dioxide by water solutions, *Journal of the Air
443 Pollution Control Association*, 17, 403–406, 1967.
- 444 Tortini, R., van Manen, S., Parkes, B., and Carn, S.: The impact of persistent volcanic degassing on vegetation: A case study
445 at Turrialba volcano, Costa Rica, *International journal of applied earth observation and geoinformation*, 59, 92–103, 2017.
- 446 Tzortziou, M., Herman, J. R., Cede, A., Loughner, C. P., Abuhassan, N., and Naik, S.: Spatial and temporal variability of
447 ozone and nitrogen dioxide over a major urban estuarine ecosystem, *Journal of Atmospheric Chemistry*, 72, 287–309, 2015.
- 448 Tzortziou, M., Parker, O., Lamb, B., Herman, J. R., Lamsal, L., Stauffer, R., and Abuhassan, N.: Atmospheric Trace Gas (NO2
449 and O3) variability in South Korean coastal waters, and implications for remote sensing of coastal ocean color dynamics,
450 *Remote Sensing*, 10, 1587, 2018.
- 451 Xi, X., Johnson, M. S., Jeong, S., Fladeland, M., Pieri, D., Diaz, J. A., and Bland, G. L.: Constraining the sulfur dioxide
452 degassing flux from Turrialba volcano, Costa Rica using unmanned aerial system measurements, *Journal of Volcanology and
453 Geothermal Research*, 325, 110–118, 2016.
- 454 Zhang, Q., Tie, X., Lin, W., Cao, J., Quan, J., Ran, L., and Xu, W.: Variability of SO2 in an intensive fog in North China Plain:
455 Evidence of high solubility of SO2, *Particuology*, 11, 41–47, 2013.
- 456 Zhang, R., Wang, G., Guo, S., Zamora, M. L., Ying, Q., Lin, Y., Wang, W., Hu, M., and Wang, Y.: Formation of urban fine
457 particulate matter, *Chemical reviews*, 115, 3803–3855, 2015.
- 458 Zhang, X. and Schreifels, J.: Continuous emission monitoring systems at power plants in China: Improving SO2 emission
459 measurement, *Energy Policy*, 39, 7432–7438, 2011.

460